Korean J. Chem. Eng., 37(8), 1401-1410 (2020)
DOI: 10.1007/s11814-020-0592-4

pISSN: 0256-1115
eISSN: 1975-7220

In situ exsolution of Rh nanoparticles on a perovskite oxide surface: Efficient Rh catalysts for Dry reforming

Emilio Audasso*,‡, Yoondo Kim,***,‡, Junyoung Cha**,****, Viviana Cigolotti*****, Hyangsoo Jeong**, Young Suk Jo**, Yongmin Kim**, Sun Hee Choi**, Sung Pil Yoon**, Suk Woo Nam**, and Hyuntae Sohn**,†**

*PERT, DICCA, University of Genova, Via Opera Pia 15, Genova 16145, Italy
**Center for Hydrogen and Fuel Cell Research, Korea Institute of Science and Technology (KIST), Seongbuk-gu, Seoul 02792, Korea
***Green School, Korea University, Seongbuk-gu, Seoul 02841, Korea
****Department of Chemical and Biological Engineering, Korea University, Seongbuk-gu, Seoul 02841, Korea
*****ENEA-Italian National Agency for New Technologies, Energy and Sustainable Economic Development, Lungotevere Thaon di Revel 76, Rome 00196, Italy
(*Received 29 March 2020 • Revised 17 May 2020 • 27 May 2020*)

Abstract−The catalytic activity of the Rh-exsolved $Sr_{0.92}Y_{0.08}Ti_2O_{3-\delta}$ perovskite catalyst (SYTRh5) was examined for dry reforming of methane. The exsolution of the Rh nanoparticles over the SYT perovskite oxide surface was carried out under various reducing environments where the extent of Rh exsolution was significantly determined by the reduction time (4, 12, 24 h) and temperature (800, 900, 1,000 °C). STYRh5 catalysts treated at a longer reduction time and a higher reduction temperature revealed formation of larger metallic Rh nanoparticles on the perovskite oxide with higher surface concentration. For dry reforming activity, the SYTRh5 catalysts reduced at 900 and 1,000 °C for 24 h showed significantly higher methane conversion compared to others. The high catalytic performance of the SYTRh5 (900 and 1,000 °C, 24 h) catalysts was attributed to the high coke-resistance of the larger Rh-exsolved nanoparticles and stronger anchoring sites resulted from the exsolution process. Post-analysis TEM images exhibited limited carbon deposition and particle agglomeration of Rh over the SYTRh5 (900 and 1,000 °C, 24 h) catalysts. Lastly, in-situ H_2S poisoning was conducted to examine the regeneration ability of SYTRh5. Although catalyst deactivation was observed, the catalytic activity of SYTRh5 (900 and 1,000 °C, 24 h) was completely recovered to the original level once the H_2S flow was interrupted, indicating facile desorption of sulfur species from the Rh-exsolved nanoparticles.

Keywords: Rh Catalysts, In Situ Exsolution, Perovskite, Dry Reforming, Hydrogen Production

INTRODUCTION

High-temperature fuel cells, such as solid oxide and molten carbonate fuel cells, have been extensively utilized for large-scale power generation [1,2]. Owing to their increasing attention in the literature, the recent studies on high-temperature fuel cells have focused not only on the development of novel materials to increase the fuel cell performance [3-7] by kinetic modeling [8-10], but also on their use in integrated power systems [11-14]. A main advantage of the high-temperature fuel cells is their high operating temperature, which allows for the direct utilization of hydrocarbon fuels that increases the total energy efficiency of the fuel cell. Among the variety of products obtained from feedstocks, biogas, which mainly consists of methane and carbon dioxide, can be directly fed at the anode side of the high-temperature fuel cells to produce hydrogen through dry reforming, eventually leading to power generation [15,16].

$$CH_4+CO_2 \rightleftharpoons 2H_2+2CO \qquad (\Delta H^o=247\ kJ/mol) \qquad (1)$$

The utilization of biogas is considered environmentally friendly as it reduces the carbon dioxide levels in the atmosphere due to the closed carbon loop. Besides, in combination with the internal reformer of the high-temperature fuel cells, the dry reforming process could also be applied for on-board power generation. However, a major obstacle for dry reforming is the larger extent of carbon deposition that severely deactivates the catalytic activity compared to the steam reforming process [17]. This issue can be alleviated by increasing the reaction temperature, but also increases the overall operation costs. Furthermore, sulfur species is often present in the biogas mixture at ppm levels. Although its concentration is extremely low, the presence of the sulfur poison in the feed deactivates the catalyst as well and ultimately deteriorates the fuel cell life cycle [18].

In recent years, metal-exsolved perovskite catalysts have attracted considerable interest in the catalysis field, owing to their strong metal-support interaction and the high dispersibility of their nanoparticles on the perovskite oxide surface. The formation of exsolved nanoparticles results from a phenomenon where the B-sites of the perovskite oxides (structure: ABO_3) are first substituted by transition metals (e.g., Ru, Rh, Ni, etc.) under oxidizing conditions, and then released (exsolved) as metal nanoparticles when exposed to a reducing atmosphere [19]. These surface-exsolved nanoparticles have great advantages over the conventional impregnated material-based cat-

†To whom correspondence should be addressed.
E-mail: sohn@kist.re.kr
‡These authors have contributed equally.

alysts. For example, Wei et al. [20] compared two different Ni supported on $LaMnO_3$-based perovskite catalysts, one was synthesized by the impregnation and the other by the exsolution method. It was observed that the Ni-exsolved catalysts exhibited higher CH_4 conversion and stability at a lower extent of coking, compared with the Ni-impregnated catalysts. The high catalytic activity and stability exhibited by the former was ascribed to the high dispersion of the Ni particles, their uniform particle size distribution, and stronger Ni-surface bonds. Similarly, Neagu et al. [21] demonstrated the high coke resistance of Ni-exsolved nanoparticles supported on an LST perovskite oxide by flowing 20% CH_4/H_2 in the absence of steam. The Ni-exsolved particles were more embedded in the oxide support, and hence contained more anchoring sites connecting the metal and the perovskite surface, which resulted in a lower tendency to agglomerate or to coke. Besides, the metal-exsolved perovskite catalysts have shown great potential for many real-world applications, such as CH_4 partial oxidation [22], electrolysis of CO_2 [23], and O_2 transport membranes [24].

Various studies on CH_4 reforming have been reported in literature. Zubenko et al. [25] studied a perovskite ($LaFeO_3$)-based catalyst with exsolved Re-alloy nanoparticles that exhibited a stable and efficient CH_4 conversion (more than 90% at an operating temperature of 900 °C). Chai et al. [26] investigated a Ni-exsolved nanoparticle perovskite ($La_{0.46}Sr_{0.34}Ti_{0.9}Ni_{0.1}O_3$) with a bimodal size distribution that exhibited better and more stable results compared to the non-exsolved Ni-based catalysts, although the CH_4 conversion was low. In a previous work [27], different $LaCrO_3$-based catalysts with Ir, Co, and Rh-exsolved nanoparticles were analyzed, which exhibited a very promising performance; particularly, Ir produced over 90% CH_4 conversion at an operating temperature of 900 °C. The metal-exsolved nanoparticles were also found to be highly sulfur resistant. For instance, Papaioannou et al. [28] stated that their perovskite-based catalysts with Fe-Ni-exsolved nanoparticles exhibit higher sulfur resistance in the CO oxidation reaction compared to the commercial Ni catalysts and achieve an almost complete recovery once the poisoning is interrupted.

SYT ($Sr_{0.92}Y_{0.08}Ti_2O_{3-\delta}$)-based perovskite oxides have been used as anode constituent for solid oxide fuel cells attributed to its high electronic conductivity as well as stability under high temperatures. Recently, it was reported that facile exsolution of metal nanoparticles is feasible over non-stoichiometric SYT-based perovskites. For example, Gunsik et al. showed successful exsolution of Ni, Ru and Rh nanoparticles from SYT perovskite structure to the oxide surface using different metal loadings. Herein, we synthesized highly dispersed Rh-exsolved nanoparticles supported on the SYT ($Sr_{0.92}Y_{0.08}Ti_2O_{3-\delta}$) perovskite and investigated the catalytic activity and stability of the SYTRh5 (5% in moles of Rh) catalyst for the first time under dry reforming conditions. The recovery characteristics of SYTRh5 from sulfur poisoning were examined. Furthermore, the effect of the reduction temperature and time on the extent of Rh exsolution over the SYT perovskite was examined not only to understand how the degree of Rh exsolution affects the catalytic activity of SYTRh5 but also to identify the optimum reduction temperature and time for dry reforming. Finally, the chemical and physical properties of the catalyst were examined by various techniques, such as temperature-programmed reduction (TPR), X-ray diffraction (XRD), X-ray photoelectron spectroscopy (XPS), and transmission electron microscopy (TEM).

EXPERIMENTAL

1. Catalyst Preparation

The $Sr_{0.92}Y_{0.08}Ti_{1.95}Rh_{0.05}O_{3-\delta}$ perovskite catalyst powders (SYTRh5) were prepared using Pechini's method, which has been reported in previous studies [29-31]. This is a type of sol-gel synthesis technique that is frequently employed to obtain well-dispersed metal ions entrapped in a covalent polymer network through an esterification of citric acid with ethylene glycol. Once the polymer matrix was removed by thermal treatment, a highly homogeneous complex metal oxide was obtained. The first step of the synthesis involved the preparation of the following three solutions: 1) yttrium nitrate [$Y(NO_3)_3{\cdot}6H_2O$ (Junsei), 0.502 g] and strontium nitrate [$Sr(NO_3)_3$ (Sigma-Aldrich), 3.191 g] in 100 g of deionized water, 2) titanium isopropoxide [$Ti(OCH(CH_3)_2)_4$ (Junsei), 9.085 g] dissolved in 100 g of ethylene glycol, and 3) rhodium chloride hydrate [$RhCl_3{\cdot}xH_2O$ (Alfa Aesar), 0.198 g] and citric acid [$C_6H_8O_7$ (Sigma-Aldrich), 100 g] dissolved in deionized water. The three solutions were then slowly mixed in a beaker at 80 °C, resulting in the formation of a precipitate. The resulting solution along with the precipitate was dried at 110 °C overnight to facilitate gelation and was subsequently calcined at 300 °C for 6 h under air to remove any remaining organic species. After grinding, the solids were ground and subsequently calcined once more at 650 °C for 10 h in air to obtain the SYTRh5 perovskite powder (5 g). For comparison, a reference SYT perovskite was prepared without adding the Rh precursor during the synthesis procedure. The exsolution of Ni [30], Ru [31], or Rh [29] over the SYT support has been previously reported in the literature. In this study, the exsolution of the Rh particles over SYTRh5 catalyst was conducted ex-situ, at different reduction temperatures and times, under a flux of $H_2 : N_2$ in the ratio 40 : 60 (80 mL/min) in a heating furnace. The samples reduced at 800, 900, and 1,000 °C for 24 h have been represented as SYTRh5 (800), SYTRh5 (900), and SYTRh5 (1000), while the samples reduced at 900 °C for 4, 8, and 12 h have been represented as SYTRh5 (4), SYTRh5 (8), and SYTRh5 (12), respectively.

2. Catalyst Characterization

2-1. Brunauer-Emmett-Teller (BET) Surface Area, Pore Volume and Pore Size

The structural information, including BET surface area, pore volume and pore size of the SYTRh5 catalysts, was obtained using N_2 physisorption technique in a Micromeritics ASAP2000 (accelerated surface area & porosimetry system) instrument. Depending on the expected surface area, a known amount of catalyst was first measured and transferred to a sample tube. The sample tube was exposed to a vacuum environment where the catalyst was degassed at 70 °C for 2 hr and 250 °C for 12 hr to remove impurities on the catalyst surface. The sample tube was then moved to the analysis port and N_2 physisorption was carried out at 77 K. The Barrett-Joyner-Halenda (BJH) pore size distribution was constructed based on the desorption branch of the isotherm.

2-2. Temperature-Programmed Reduction (TPR)

The BELCAT-M chemisorption analyzer, MicrotracBEL Corp.,

was used to conduct the TPR of the SYTRh5 catalysts. The sample was placed in a quartz reactor tube equipped with a thermocouple to monitor the temperature of the catalyst bed. Pure Ar at a flowrate of 70 mL/min was introduced into the reactor at 25 °C and the reactor temperature was increased to 250 °C. The sample was pretreated for 2 h to eliminate the adsorbed water on the catalyst surface. The temperature of the reactor was then decreased to room temperature while continuing the flow of pure Ar. For the TPR, 70 mL/min of 5% H_2/Ar was used and the temperature of the reactor was increased from 50 to 900 °C at a ramp rate of 10 °C/min. The outstream of the reactor was connected to a thermal conductivity detector (TCD) to estimate the hydrogen consumed by the catalyst.

2-3. X-ray Diffraction (XRD)

X-ray diffraction (XRD) patterns of the as-prepared SYTRh5 catalysts powders and of the samples reduced under different conditions of time and temperature were collected using a MiniFlex II diffractometer (Rigaku Co.) with CuKα radiation (wavelength λ= 1.5418 Å). The diffraction patterns were collected in the 2θ range of 20°-90° and the crystallographic phases were identified using the PDXL software.

2-4. Transmission Electron Microscopy (TEM)

To analyze the morphology of the studied catalyst powders, TEM images were recorded using a TEM Tecnai F20 (FEI Co.) equipped with a high-brightness field-emission electron gun (FEG) operated at 200 kV. Before conducting the analysis, the catalyst powders were suspended in ethanol and sonicated for 15 min to obtain a homogeneous mixture. A single drop placed on a grid was used to investigate the morphology of the powders.

2-5. X-ray Photoelectron Spectroscopy (XPS)

To confirm the presence of Rh on the surface of the catalyst powders, X-ray photoelectron spectroscopy (XPS) spectra were recorded using a K-Alpha+ XPS System (Thermo Scientific Co.). The samples were loaded into the chamber using carbon tape and the chamber was evacuated for 2.5 h. A survey scan was conducted for each sample to identify all the elements present on the surface of the powders. Subsequently, the spectra for the specific C 1s, O 1s, Ti 2p, Y 3d, Sr 3d, and Rh 3d regions were recorded. Prior to the data analysis, the charging effect was corrected based on the C 1s binding energy of 284.5 eV.

3. Catalytic Activity under Dry Reforming Conditions

The dry reforming activity of the SYTRh5 catalysts was tested under atmospheric pressure in a fixed-bed vertical quartz reactor. The gas flow was fed into the top of the tube while the bottom served as an exhaust line, which was directly connected to a gas chromatograph (GC). To ensure that no water could reach the GC, the outlet stream was cooled to a temperature of 4 °C. The catalyst bed was placed in the middle of the tube and 0.2 g of a catalyst sample was used for each test. The composition of the dry off-gas was measured using a GC with a TCD and two separation columns. We plotted Q and molecular sieve (both 30 m in length), using He and Ar, respectively, as carrier gases to determine the concentrations of H_2, CO, CO_2, and CH_4.

The feed consisted of a CH_4 : CO_2 : N_2 mixture at a ratio of 1 : 1 : 2 and a total flow rate of 80 mL/min. The gas hourly space velocity was 1.2×10^4 h^{-1}. All samples of the reduced SYTRh5 catalyst prepared as described in Section 2.1 were once more reduced in situ using the same reduction procedure (catalyst preparation) prior to the dry reforming reaction, except for the sample reduced at 1,000 °C (as this exceeds the temperature limit of the reaction testing furnace). Dry reforming of methane was carried out in the temperature range of 600 to 900 °C with temperature increments of 50 °C. The reaction was carried out for 2 h at each temperature, while multiple GC injections were made. Once the prereduction was complete, the reaction temperature was adjusted to 900 °C and the reaction was carried out from 900 to 600 °C. Then, the activity testing was repeated from 600 to 900 °C to investigate the thermal cycling stability of the catalysts. Finally, for the H_2S recovery testing, a H_2S 400 PPM calibration gas balance N_2 cylinder was used; additional N_2 was added to the reactant to obtain 100 ppm of H_2S. Overall, a mixture of H_2S, CH_4, CO_2, and N_2 was introduced into the catalyst bed for a prolonged time over the SYTRh5 reduced at different reduction temperatures and times. Once the H_2S poisoning was completed, the inlet for H_2S was closed to observe whether the catalyst could recover its original activity.

To examine the performance of the catalysts, we referred to the conversion rate of CH_4 and CO_2, and the ratio between the produced H_2 and CO. To evaluate these numbers, the following equations were used:

$$\text{Methane Conversion} = \frac{n_{CH_4,\,in} - n_{CH_4,\,out}}{n_{CH_4,\,in}} \quad (2)$$

$$\text{Carbon Dioxide Conversion} = \frac{n_{CO_2,\,in} - n_{CO_2,\,out}}{n_{CO_2,\,in}} \quad (3)$$

$$H_2/CO = \frac{n_{H_2,\,out}}{n_{CO,\,out}} \quad (4)$$

RESULTS AND DISCUSSION

1. In Situ Growth of Rh Nanoparticles on the SYT Surface

The SYTRh5 catalysts must undergo a reduction process to exsolve the substituted Rh from the perovskite structure such that Rh nano-

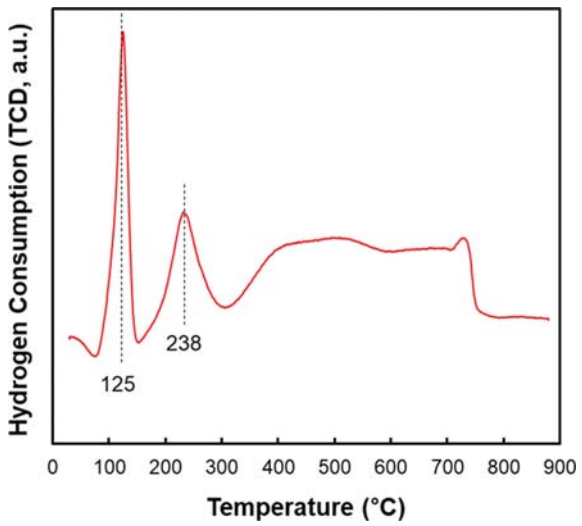

Fig. 1. TPR Profile of SYTRh5 catalysts (exsolution of Rh).

particles are homogenously dispersed on the surface. Initially, a TPR experiment was conducted to understand the exsolution behavior of SYTRh5 at different reduction temperatures. As shown in Fig. 1, multiple reduction peaks are observed, especially near the low temperature region. The first peak was assigned to the surface RhO*x* species that were not incorporated into the perovskite structure, and therefore, remained on the catalyst surface. The intensity of this peak reportedly increases with high Rh loading, indicating that the substitution of the Ti sites to Rh is limited to some extent, leading to the formation of non-exsolved surface Rh nanoparticles [29]. The second peak of the TPR profile indicates the exsolution of Rh particles that are present in the vicinity of the catalyst surface. The substituted Rh cations that are located near the surface of the perovskite structure are considered to have lesser diffusion restriction for moving toward the surface compared with the bulk Rh species, thus exhibiting a high degree of exsolution at relatively lower temperatures. On the other hand, a broad peak is observed between 300 to 800 °C, which is linked to the bulk Rh exsolution. The bulk Rh reduction takes place at much higher temperatures and at a wider temperature range. This demonstrates that higher temperatures and longer reduction times are possibly required to completely exsolve the Rh species from the B sites of the perovskite lattice structure. Incomplete exsolution of Rh due to short reduction time and low reduction temperature can significantly influence the catalytic activity of SYTRh5 for dry reforming, resulting in inconsistent catalytic performance. Therefore, in this study, the effect of the reduction temperature and time on the extent of Rh exsolution and catalytic performance of the SYTRh5 was investigated to identify the most adequate reaction conditions for dry reforming.

2. Effect of Reduction Time

2-1. Physical Properties of SYTRh5 Catalysts

The BET surface area, pore volume and average pore size over SYTRh5 catalysts are shown in Table 1. Compared to the as-prepared sample, all these values decrease significantly after the reduction process, possibly indicating that Rh exsolution well took place at the inner pores of the SYT perovskite structure. With respect to reduction temperature and time, similar surface area, pore volume and pore size were obtained over the SYTRh5 catalysts reduced at 900 °C and 1,000 °C except SYTRh5 (800) due to lower reduction temperature.

2-2. Particle Size of Rh and Extent of Exsolution

The TEM images of the SYTRh5 catalysts reduced at different reduction times were collected to confirm the exsolution of the Rh nanoparticles from the SYT perovskite oxide. Fig. 2 shows the SYTRh5 sample before (a) and after the reduction performed for 4 h (b), 12 h (c) and 24 h (d), at the same temperature of 900 °C. The following observations are made: First, as compared to the non-reduced SYTRh5 sample, the sintering level of the SYT support

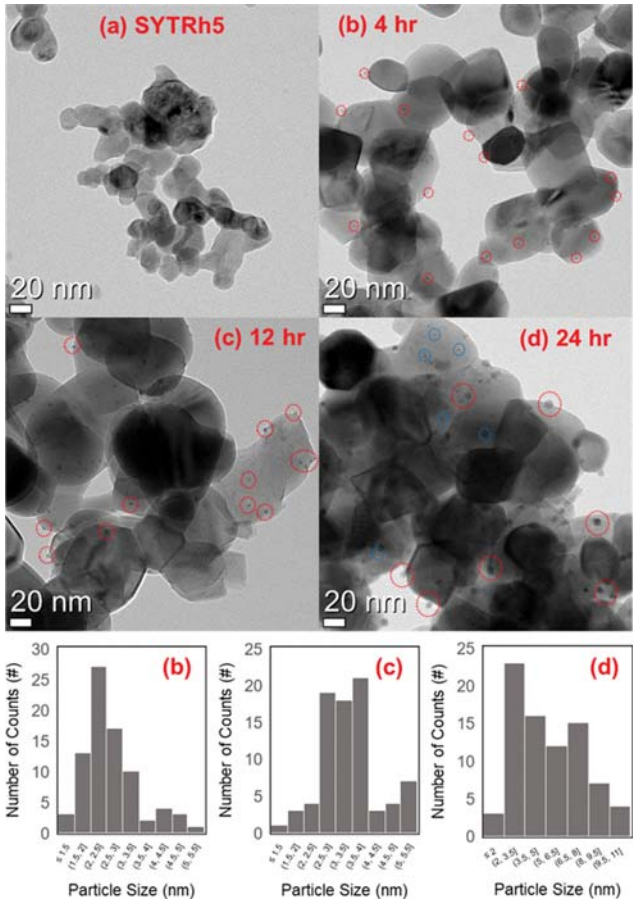

Fig. 2. TEM images of: (a) as-prepared SYTRh5 catalysts, and (b) SYTRh5 reduced at 900 °C for 4 h, (c) 12 h, and (d) 24 h for the same scale bar. The red and blue circles on the image indicate Rh-exsolved nanoparticles formed on the SYT oxide surface.

increases with the reduction time. The particle size of the SYT support increases from an average diameter of 18 nm (non-reduced) to 50 nm for SYTRh5 (4). When the reduction time is increased to 12 h, the final powders reach an average diameter of 80 nm that almost remains constant up to reduction time of 24 h.

Furthermore, the exsolution of the Rh particles to the SYTRh5 surface is observed to be greatly time dependent. With respect to the bare SYTRh5 sample, no formation of Rh particles was observed, which indicates that most of the Rh species are incorporated inside the perovskite structure after catalyst synthesis. After 4 h of reduction, the SYTRh5 (4) sample exhibits low extent of Rh exsolution, leading to segregated Rh nanoparticles on the surface with an average diameter of 2.6 nm (marked by the red circles on the TEM images). The average diameter of the Rh nanoparticles increases to 3.4 nm after 12 h of reduction, and finally reaches 5.1

Table 1. BET surface area, pore volume and pore size of the SYTRh5 catalysts reduced at X °C for Y h (X/Y)

	As-prepared	800/24	900/4	900/12	900/24	1000/24
BET surface area (m^2/g)	39.4	28.1	14.0	12.9	15.4	9.16
Pore volume (cm^3/g)	0.28	0.12	0.03	0.03	0.03	0.02
Pore size (Å)	273	165	90.6	96.8	84.0	74.4

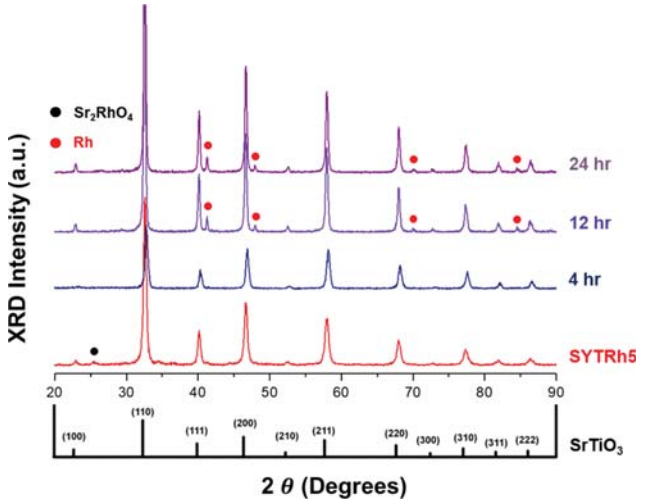

Fig. 3. Powder XRD patterns of the as-prepared SYTRh5 catalysts and SYTRh5 reduced at 900 °C for 4, 12, and 24 h. The reference $SrTiO_3$ perovskite is shown at the bottom.

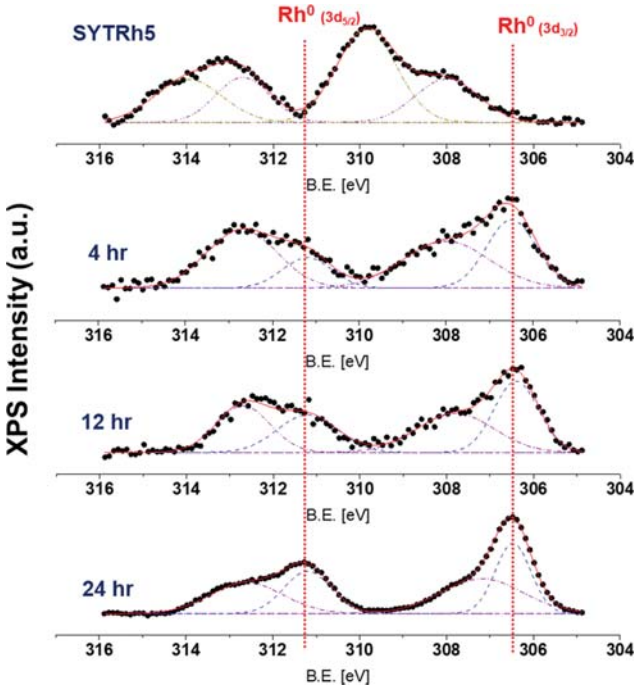

Fig. 4. XPS Rh 3d fitted spectra of the as-prepared SYTRh5 catalysts and SYTRh5 reduced at 900 °C 4, 12, and 24 h.

nm for the SYTRh5 (24) catalysts. Compared with the non-reduced SYTRh5 samples, the presence of Rh particles on the surface of the reduced catalyst samples indicates that exposing the catalyst to a reducing environment is essential to exsolve the Rh species. Interestingly, tiny Rh particles were also observed, especially on SYTRh5 (24) (Fig. 2(d), blue circles). This could be attributed to the difference between the exsolution rate of Rh in the bulk and surface and/or immobile Rh particles that are significantly more stable under high reduction temperatures compared with the others. Furthermore, the possibility of the existence of the Rh particles close to single-atom size cannot be ruled out for all tested SYTRh5 catalysts, since these sites are hardly visible in the TEM images. These results indicate that longer reduction time is required to completely exsolve most of the Rh nanoparticles to the catalyst surface.

Fig. 3 compares the XRD spectra of the SYTRh5 catalysts with the reference spectra of $SrTiO_3$ (JCPDS 35-0734). The XRD pattern of the as-prepared SYTRh5 does not show any major peaks related to the formation of byproducts such as RhO_2, except for a negligible amount of Sr_2RhO_4, suggesting that the Rh was successfully substituted in the SYT lattice. The spectrum of SYTRh5 (4) shows only the peaks related to the perovskite structure without any secondary peaks that could suggest the high stability of the perovskite structure of the SYTRh5 under harsh reducing conditions. Moreover, although approximately 2 nm Rh particles were observed in the TEM images for the SYTRh5 (4) catalyst, the size of the Rh nanoparticles was too small to be detected using XRD due to short-range ordering. On the contrary, the spectra of the SYTRh5 (12) and SYTRh5 (24) catalysts clearly show peaks related to metallic Rh and the intensity of these peaks increases as with the reduction time. This is in good agreement with the TEM results, explicitly suggesting that the extent of the exsolution is firmly dependent on the reduction time.

2-3. Oxidation States of Rh-exsolved Particles

The electronic characteristics of the SYTRh5 treated under different reduction times was examined by XPS. Fig. 4 shows the fitted Rh 3d XPS spectra of the as-prepared SYTRh5 and SYTRh5 (4, 12, 24) samples. Three doublet peaks are observed in the spectra: the doublet at 306.5 and 311.5 eV in the $3d_{3/2}$ and $3d_{5/2}$ orbitals indicates metallic Rh (Rh^0), whereas the other peaks appearing at higher binding energies are attributed to the oxidized Rh states (Rh^{x+}) [32-34]. In the case of the as-prepared SYTRh5 samples, most of the Rh species were oxidized and no formation of metallic Rh was observed on the catalyst surface. However, with longer reduction time, a significant increase was observed in the peak intensity for metallic Rh, revealing the exsolution of the Rh particles to the surface of SYTRh5 catalyst. An analysis of the relative areas shows that with increasing reduction time, the percentage of metallic Rh increased compared with the one related to the oxide (Rh metal/Rh oxide ratio is 38 : 62 after 4 h, 50 : 51 after 12 h, and 53 : 47 after 24 h) confirming its higher presence on the surface due to exsolution. Note that the resolution of the XPS spectra enhances with increasing reduction time. This is ascribed to the increasing surface concentration of Rh located on the catalyst surface, again signifying the exsolution of Rh during the reduction process.

2-4. Dry Reforming Reactivity of SYTRh5 (4, 12, 24)

The SYTRh5 (4, 12, 24) catalysts were tested for dry reforming of CH_4 in a fixed-bed reactor system by changing the operating temperature from 900 to 600 °C and again back to 900 °C at constant time intervals. The outlet gas was analyzed by GC to quantify the CH_4 conversion, and the CO, CO_2, and H_2 yield. The results are plotted in the Fig. 5(a), and the averaged CH_4 conversion values obtained from the two temperature ranges are shown in Fig. 5(b). The catalytic activity data of all the samples tested in this study are presented in Table 2. Among the catalysts reduced at different reduction times, SYTRh5 (4) exhibited significantly lower

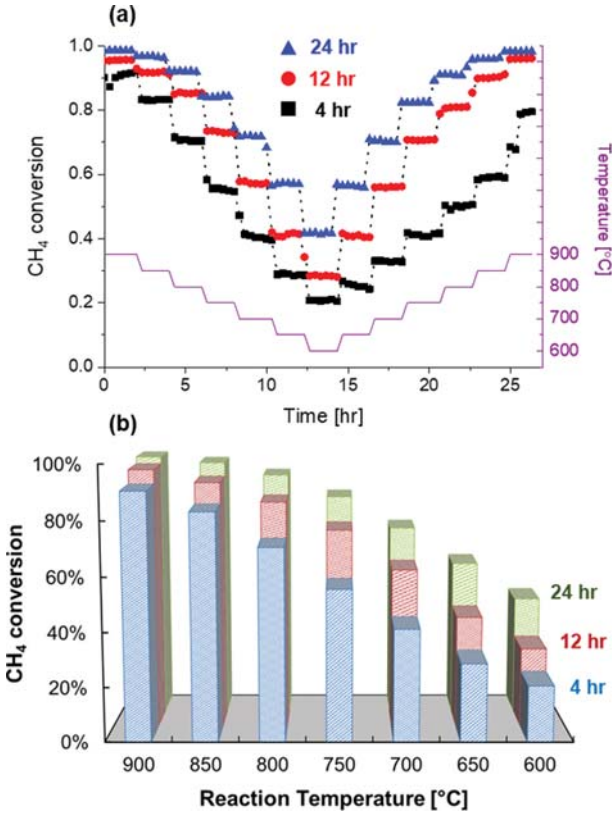

Fig. 5. Catalytic activity of SYTRh5 (4, 12, 24) catalysts under dry reforming conditions. (a) CH_4 conversion at different operating temperatures, (b) averaged CH_4 conversion obtained from thermal cycling (from 900 °C to 600 °C and back to 900 °C). It should be noted that the SYTRh5 (4) sample does not recover its original catalytic activity.

catalytic performance in the CH_4 conversion; moreover, its catalytic stability was also observed to be low. As shown in the figure, lower methane conversions are achieved over SYTRh5 (4) when the reaction was repeated at equal reaction temperatures. The deactivation of the catalyst is predominantly attributed to the significant carbon formation on the catalyst surface, which was verified in the post-catalysis analysis. Comparatively, SYTRh5 (12) exhibited a slightly better catalytic performance at all reaction temperatures; moreover, similar CH_4 conversions were obtained with increasing reaction temperature, demonstrating the high stability of the catalyst. Finally, SYTRh5 (24) exhibited the best performance, achieving close to 100% conversion at 850 °C, and exhibited complete repeatability of these results between the 600 °C and 900 °C temperature range.

The observed order of reactivity (4<12<24 h) under dry reforming conditions indicates that catalytic activity is closely related to the extent of exsolution of Rh, i.e., higher catalytic activity results in higher extent of exsolution. This is partly because dry reforming is generally operated under strong diffusion limited conditions. Therefore, with the increase in Rh concentration on the exterior surface of the SYT support, faster kinetics of the reaction is expected leading to higher conversion of CH_4. Thus, a longer reduction time results in higher surface concentration of Rh leading to increased

Table 2. Summary of dry reforming reactivity of the SYTRh5 catalysts tested in this study

SYTRh5 reduced at X °C for Y h (X/Y)					
Temperature (°C)	900/4	900/12	900/24	800/24	1000/24
(a) CH_4 conversion (%)					
600	20.7	29.2	43.8	19.4	49.1
650	27.1	41.1	57.6	25.1	66.2
700	36.9	58.8	71.3	34.5	80.6
750	50.1	73.6	83.3	49.1	90.0
800	66.5	83.9	91.5	64.6	94.9
850	81.2	91.1	96.2	81.1	97.3
900	90.8	95.8	98.4	91.6	98.3
(b) CO_2 conversion					
600	19.2	30.3	44.5	16.5	58.1
650	27.8	45.2	61.0	24.5	73.0
700	40.2	65.0	76.0	36.7	86.4
750	54.8	79.8	87.4	53.5	94.2
800	71.3	89.0	94.4	70.9	98.0
850	85.2	95.1	97.9	85.9	99.7
900	94.1	98.8	99.5	94.3	99.8
(c) H_2/CO ratio					
600	0.49	0.70	0.73	0.40	0.72
650	0.60	0.88	0.78	0.52	0.80
700	0.67	0.86	0.84	0.61	0.86
750	0.75	0.87	0.88	0.71	0.90
800	0.82	0.91	0.92	0.80	0.92
850	0.87	0.93	0.93	0.87	0.93
900	0.91	0.95	0.94	0.91	0.94

number of active sites, whereas a shorter reduction time results in lower surface concentration of Rh on the catalyst surface indicating lower catalytic activity. Another factor that should be considered is the effect of the Rh particle size. Zhang et al. [35] studied the effect of the Rh particle size on the catalytic activity of Rh on various supports such as YSZ, Al_2O_3, TiO_2, SiO_2, La_2O_3, and MgO under dry reforming conditions. The results showed a significantly faster deactivation rate as the particle size of Rh decreased from 6 to 1 nm. Particularly on Al_2O_3 and SiO_2 supports, the deactivation rate rapidly increased from a point of 2.5 nm. A similar conclusion was drawn by Ligthart and co-workers [36] who reported that Rh nanoparticles smaller than 2.5 nm deactivate faster in a steam-methane reforming reaction compared with others having 4-9 nm particles. This was attributed to the small particle size of Rh, which results in lower density of the step-edge sites; these sites are predominantly responsible for the C-O recombination that removes the deposited carbon from the catalyst surface during a methane reforming reaction. In case of the SYTRh5 (4) sample, which was fairly unstable over the thermal cycling process, the particle size of Rh was close to 2 nm. Therefore, these results are in good agreement with the previous studies, suggesting that the higher

catalytic activity of SYTRh5 reduced at higher temperatures is attributed to the higher surface concentration of the Rh particles and to their larger particle size.

3. Effect of Reduction Temperature

3-1. Results of TEM, XRD, and XPS

In addition to the reduction time, the effect of the reduction temperature on the catalytic activity of SYTRh5 was examined. For this study, the reduction time was fixed at 24 h to ensure that most of the Rh atoms exsolved to the catalyst surface. The TEM images of the as-prepared SYTRh5 catalysts and samples reduced at 800 °C (b), 900 °C (c), and 1,000 °C (d) are shown in Fig. 6. Based on the TPR results, reduction temperatures lower than 800 °C have not been considered. As shown in Fig. 6, the increase in the reduction temperature significantly affects the particle size and number of nanoparticles exsolved to the catalyst surface. Furthermore, the average diameters of the SYT support vary from 40 nm (at 800 °C) to 50 nm (at both 900 °C and 1,000 °C), while the size of the Rh nanoparticles increases from an average of 2.6 nm for SYTRh5 (800) to 5.2 nm for those reduced at 1,000 °C. The particle sizes of SYTRh5 (900) and SYTRh5 (1000) are comparable, which indicates that the Rh-exsolved particles with sizes close to 10 nm are reasonably stable at this temperature range, although a higher number of Rh particles were observed in the same region of the TEM images over the SYTRh5 (1000) catalyst. These results again clearly indicate that the temperature of the reducing environment is important in order to improve the extent of the Rh exsolution as well as to control the sintering level of the Rh particles.

The XRD spectra of the SYTRh5 reduced at different temperatures are shown in Fig. 7. As expected, SYTRh5 (800) shows only the peaks related to the perovskite structure, owing to the extremely

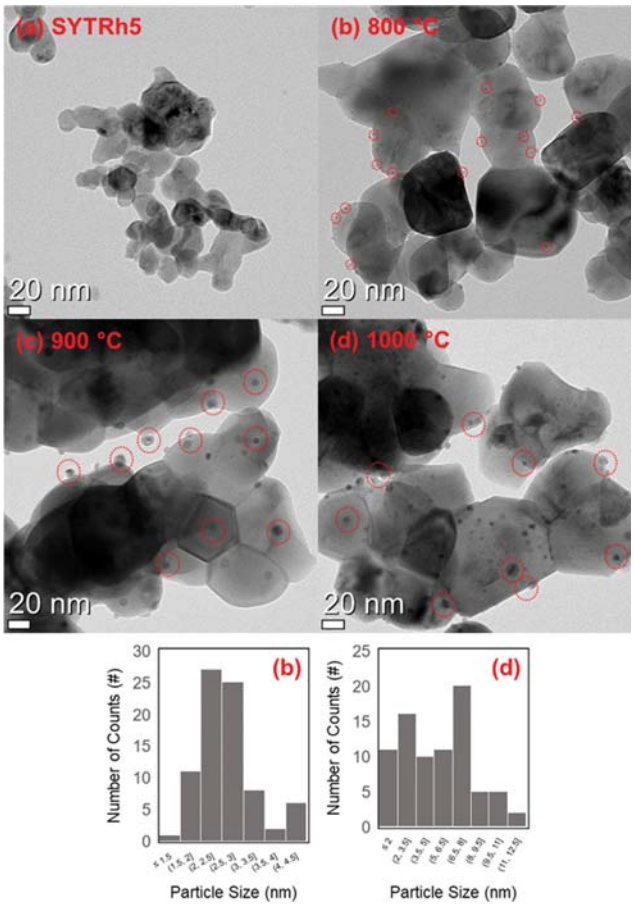

Fig. 6. TEM images of the (a) as-prepared SYTRh5 catalysts, and (b) SYTRh5 reduced for 24 h at 800 °C, (c) 900 °C, and (d) 1,000 °C at the same scale bar. The red circles on the image indicate the Rh-exsolved nanoparticles formed on the SYT oxide surface. Particle size for (c) 900 °C, 24 h can be found in Fig. 2(d).

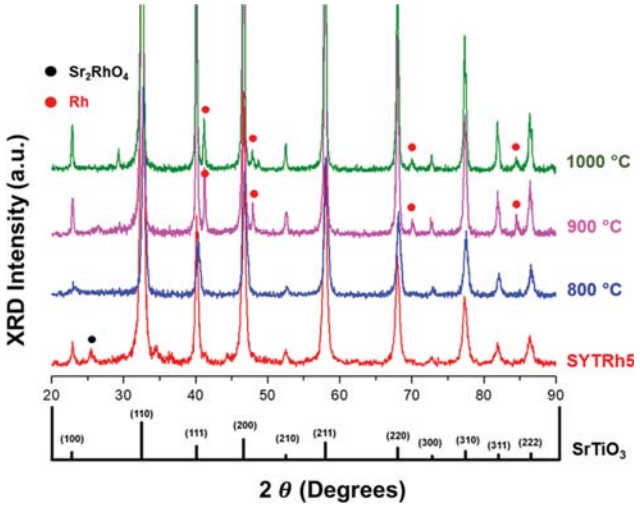

Fig. 7. Powder XRD patterns of the as-prepared SYTRh5 catalysts and SYTRh5 reduced for 24 h at 800, 900, and 1,000 °C. The reference $SrTiO_3$ perovskite is shown at the bottom.

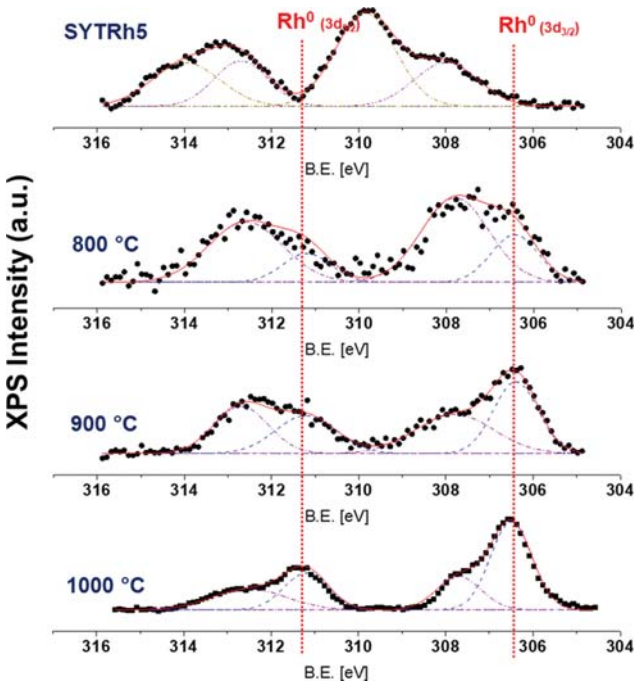

Fig. 8. XPS Rh 3d fitted spectra of the as-prepared SYTRh5 catalysts and SYTRh5 reduced for 24 h at 800, 900, and 1,000 °C.

small size of its Rh nanoparticles, while the SYTRh5 (900, 1000) catalysts reveal peaks assigned to metallic Rh, indicating the exsolution of Rh from the bulk perovskite structure in the form of Rh nanoparticles on the surface, as shown in the TEM images. A similar conclusion can also be drawn from the XPS spectra. The fitted Rh 3d XPS spectra of the SYTRh5 catalysts after reduction at 800, 900, and 1,000 °C are shown in Fig. 8. As mentioned in the previous Section 3.2.2, the binding energies of 306.5 and 311.5 eV can be attributed to metallic Rh [34]. An analysis of the relative areas shows that with increasing reduction temperature, the percentage of metallic Rh increases, confirming its higher concentration on the surface due to exsolution. Furthermore, the intensity of the Rh 3d XPS spectra significantly increases, as observed previously in the section 3.2, indicating that a higher surface concentration of Rh is observed when reduced at higher temperatures.

3-2. Dry Reforming Activity of SYTRh5 (800, 900, 1000)

Dry reforming of methane was carried out to investigate the effect of reduction temperature on the catalytic activity of the SYTRh5 samples. The reaction conditions and procedures are described in Section 3.2.4, and the following observations were made: First, as shown in Fig. 9(a), higher CH_4 conversions are obtained by SYTRh5 catalysts that have been reduced at higher temperatures. For example, the SYTRh5 (900, 1000) catalysts exhibit considerably higher CH_4 conversions compared with SYTRh5 (800) at the same temperature (600 °C). As the operating temperature increases, this difference of CH_4 conversion decreases, and close to complete conversion of CH_4 is achieved by all catalysts. The greater catalytic activity of SYTRh5 (900, 1000) is due to the higher surface concentration of Rh through exsolution from the perovskite oxide. This indicates that not only the reduction time but also the reduction temperature determines the performance of the catalysts from the following aspects: 1) surface concentration of Rh nanoparticles, 2) particle size of Rh, and 3) metal-support interaction by facilitating exsolution of Rh. Finally, thermal cycling tests were carried out to examine the stability of these catalysts by varying the reaction temperature from 900 to 600 °C and repeating the experiment from 600 to 900 °C. Both the SYTRh5 (900, 1000) catalysts showed excellent stability, whereas SYTRh5 (800) reached to slightly lower CH_4 conversion when the reaction was repeated at identical temperatures.

Lastly, TEM imagining was conducted on the SYTRh5 catalysts that were collected after dry reforming to identify the primary cause for catalyst deactivation over time in a qualitative manner. In Fig. 10, the TEM images of the post-catalysis SYTRh5 samples after 4 h (a), 12 h (b), and 24 h (c) reduction at 900 °C, and after 24 h reduction at 1,000 °C (d) are presented. To increase the randomness of the experiment, the images were taken at multiple spots across the sample specimen. The formation of carbon species is observed in all four cases; however, with increasing reduction time and temperature, the carbon coking was significantly limited. The high resistance to coke formation could be attributed to the stronger metal-support interaction of the exsolved SYTRh5 catalyst, which is not easily achievable over the conventional metal-deposited catalysts. Neagu et al. [21] reported nano-socketed Ni particles grown through exsolution, which are highly coke-resistant under methane reforming conditions. The authors stated that because these nickel particles are socketed into the perovskite sur-

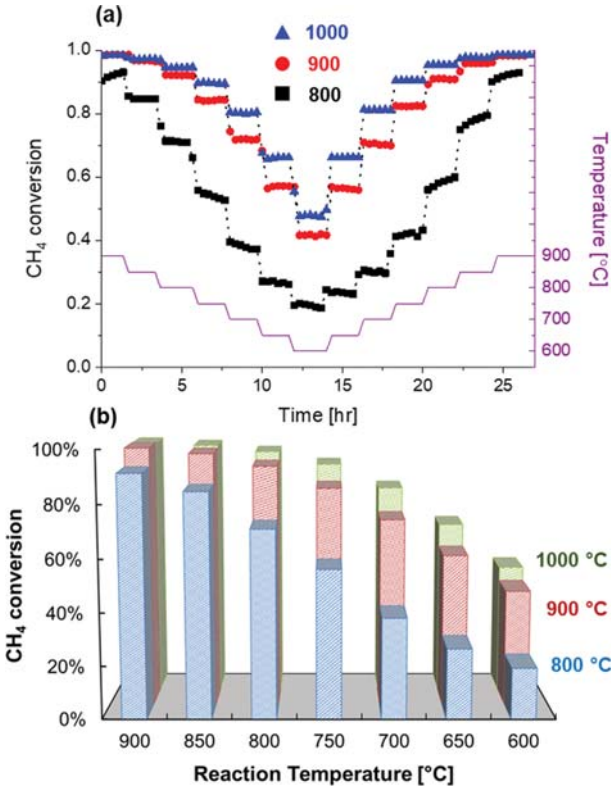

Fig. 9. Catalytic activity of SYTRh5 (800, 900, 1000) catalysts under dry reforming conditions. (a) CH_4 conversion at different operating temperatures, (b) averaged CH_4 conversion obtained from thermal cycling (from 900 to 600 °C and back to 900 °C).

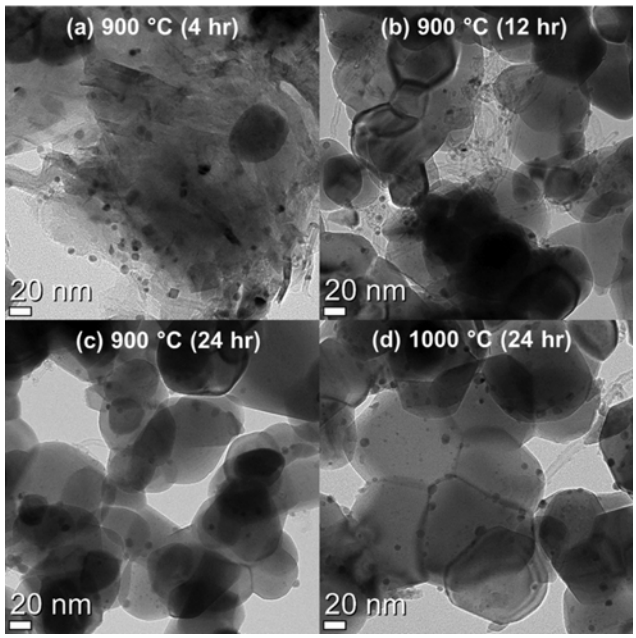

Fig. 10. TEM images of the SYTRh5 catalysts after dry-reforming activity tests (a) SYTRh5 (4, 900), (b) SYTRh5 (12, 900), (c) SYTRh5 (24, 900), (d) SYTRh5 (24, 1000).

face, "base growth" carbon coking is preferred. This growth mechanism, instead of lifting the metal particles upwards, leads to a carbon formation that is horizontal to the surface; this is due to the significantly strong adhesion between the metallic phase and the support. Regarding the SYTRh5 catalyst, the high coke resistance of the SYTRh5 (24, 900) and SYTRh5 (24, 1000) catalysts is therefore possibly attributed to the formation of larger Rh-exsolved particles whose Rh particles are significantly more attached to the SYT support, leading to a stronger metal-support interaction. Furthermore, limited agglomeration of the Rh-exsolved particles was observed over the SYTRh5 (24, 900) and SYTRh5 (24, 1000) catalysts, whereas for SYTRh5 (4, 900) and SYTRh5 (12, 900), the size of the Rh-exsolved particles increased after dry reforming.

4. Recovery of Catalytic Activity of the SYTRh5 after Sulfur Poisoning

The recovery characteristics of SYTRh5 from sulfur poisoning was investigated by flowing a mixture of H_2S, CH_4 and CO_2 into the reactor at 900 °C. The following three samples were subjected to the testing: SYTRh5 (24, 800), SYTRh5 (24, 900), and SYTRh5 (24, 1000). For this experiment, the reduction time was fixed at 24 h for comparison. As displayed in Fig. 11, the CH_4 conversion by catalysts reduced at different reduction temperatures significantly decrease on the introduction of H_2S into the reactant stream. This was fairly expected considering the high concentration of H_2S. Although, all three catalyst were severely deactivated under H_2S conditions, the SYTRh5 (24, 1000) showed slightly higher CH_4 conversion of 29%. When the H_2S feed was interrupted, a complete regeneration of the catalyst was achieved in both cases of SYTRh5 (24, 900), and SYTRh5 (24, 1000), and the CH_4 conversions quickly returned to the original level. On the other hand, the SYTRh5 (24, 800) catalyst could not recover its original activity even after a few hours of reaction revealing limited recovery, producing a conversion of about 75%. Note that all three catalysts deactivated under H_2S conditions. The remarkably high recovery rate of the SYTRh5 (900, 1000) catalysts is attributed to the higher degree of exsolution of the Rh particles, which is a result of the higher reduction temperature, that are strongly anchored to the SYT catalyst support. This strong synergy effect between the metallic Rh and SYT support possibly increases the electron deficiency of the active sites, thereby lowering the desorption energy of the sulfur species to the metal.

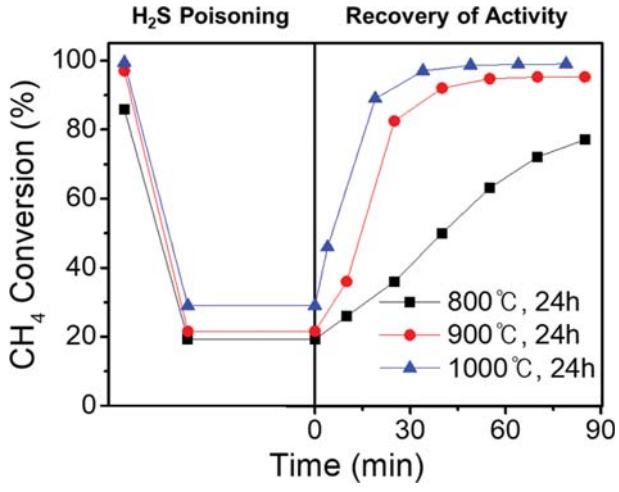

Fig. 11. H_2S poisoning and recovery test results of SYTRh5 (800, 900, 1000 reduced for 24 h) catalysts at operating temperature of 900 °C for dry reforming.

CONCLUSIONS

Rh-exsolved nanoparticles on a $Sr_{0.92}Y_{0.08}Ti_2O_{3-\delta}$ perovskite oxide were synthesized (SYTRh5) and their catalytic activity was investigated for dry reforming. It was found that the extent of exsolution of the Rh nanoparticles from the SYT perovskite framework was strongly dependent on the reduction time (4, 12, 24 h) and temperature (800, 900, 1,000 °C). The SYTRh5 catalyst pre-treated at a longer reduction time and a higher reduction temperature revealed greater extent of in situ Rh exsolution that resulted in larger Rh-exsolved nanoparticles on the catalyst surface, and higher surface concentration of metallic Rh. The SYTRh5 catalysts reduced at 900 and 1,000 °C for 24 h exhibited significantly better catalytic performances under dry reforming conditions compared to others. This was attributed to the larger Rh-exsolved nanoparticles that were partially embedded into the perovskite framework, leading to a stronger metal support interaction with higher coke resistance. The TEM images of the post-catalysis SYTRh5 (900 and 1,000 °C, 24 h) confirmed limited carbon growth over the perovskite oxide surface under dry reforming conditions. Lastly, complete recovery of SYTRh5 (900 and 1,000 °C, 24 h) activity was achieved after exposing the catalysts to 100 ppm of H_2S, indicating the facile desorption of sulfur species from the Rh-exsolved nanoparticles.

ACKNOWLEDGEMENTS

This work was supported by the Global Research Laboratory Program (Grant Number NRF-2009-00406) funded by the Ministry of Education, Science and Technology of Korea and the Hydrogen Energy Innovation Technology Development Program of the National Research Foundation of Korea (NRF) funded by the Korean government (Ministry of Science and ICT(MSIT)) (No. 2019M3E6A1104113).

REFERENCES

1. M. Minutillo, A. Perna and E. Jannelli, *Int. J. Hydrogen Energy*, **39**, 21688 (2014).
2. A. Permatasari, P. Fasahati, J.-H. Ryu and J. J. Liu, *Korean J. Chem. Eng.*, **33**, 3381 (2016).
3. Y. Huan, Y. Li, B. Yin, D. Ding and T. Wei, *J. Power Sources*, **359**, 384 (2017).
4. D. Frattini, G. Accardo, A. Moreno, S. P. Yoon, J. H. Han and S. W. Nam, *J. Ind. Eng. Chem.*, **56**, 285 (2017).
5. I. Shajahan, J. Ahn, P. Nair, S. Medisetti, S. Patil, V. Niveditha, G. U. B. Babu, H. P. Dasari and J.-H. Lee, *Mater. Chem. Phys.*, **216**, 136 (2018).
6. L. Spiridigliozzi, G. Dell'Agli, A. Marocco, G. Accardo, M. Pansini, S. P. Yoon, H. C. Ham and D. Frattini, *J. Ind. Eng. Chem.*, **59**, 17

(2018).
7. E. Pikalova, A. Kolchugin, E. Filonova, N. Bogdanovich, S. Pikalov, M. Ananyev, N. Molchanova and A. Farlenkov, *Solid State Ionics*, **319**, 130 (2018).
8. C. Li, Y. Shi and N. Cai, *J. Power Sources*, **195**, 2266 (2010).
9. E. Arato, E. Audasso, L. Barelli, B. Bosio and G. Discepoli, *J. Power Sources*, **330**, 18 (2016).
10. T. Y. Kim, B. S. Kim, T. C. Park and Y. K. Yeo, *Korean J. Chem. Eng.*, **35**, 118 (2018).
11. P. Sarmah and T. K. Gogoi, *Energy Convers. Manage.*, **132**, 91 (2017).
12. Y. Patcharavorachot, D. Saebea, S. Authayanun and A. Arpornwichanop, *Int. J. Hydrogen Energy*, **43**, 17821 (2018).
13. Q. Hou, H. Zhao and X. Yang, *Energy*, **150**, 434 (2018).
14. L. Barelli, G. Bidini and A. Ottaviano, *Energy*, **118**, 716 (2017).
15. T. Tagawa, A. Yanase, S. Goto, M. Yamaguchi and M. Kondo, *J. Power Sources*, **126**, 1 (2004).
16. W.-J. Jang, Y.-S. Jung, J.-O. Shim, H.-S. Roh and W. L. Yoon, *J. Power Sources*, **378**, 597 (2018).
17. O. Shtyka, M. Zakrzewski, R. Ciesielski, A. Kedziora, S. Dubkov, R. Ryazanov, M. Szynkowska and T. Maniecki, *Korean J. Chem. Eng.*, **37**, 209 (2020).
18. K.-J. Lee, S. Koomson and C.-G. Lee, *Korean J. Chem. Eng.*, **36**, 600 (2019).
19. D. Neagu, G. Tsekouras, D. N. Miller, H. Ménard and J. T. S. Irvine, *Nat. Chem.*, **5**, 916 (2013).
20. T. Wei, L. Jia, H. Zheng, B. Chi, J. Pu and J. Li, *Appl. Catal. A: Gen.*, **564**, 199 (2018).
21. D. Neagu, T.-S. Oh, D. N. Miller, H. Ménard, S. M. Bukhari, S. R. Gamble, R. J. Gorte, J. M. Vohs and J. T. S. Irvine, *Nat. Commun.*, **6**, 8120 (2015).
22. R. Palcheva, U. Olsbye, M. Palcut, P. Rauwel, G. Tyuliev, N. Velinov and H. H. Fjellvåg, *Appl. Surf. Sci.*, **357**, 45 (2015).
23. S. Park, Y. Kim, H. Han, Y. S. Chung, W. Yoon, J. Choi and W. B. Kim, *Appl. Catal. B: Environ.*, **248**, 147 (2019).
24. D. Papargyriou, D. N. Miller and J. T. S. Irvine, *J. Mater. Chem. A*, **7**, 15812 (2019).
25. D. Zubenko, S. Singh and B. A. Rosen, *Appl. Catal. B: Environ.*, **209**, 711 (2017).
26. Y. Chai, Y. Fu, H. Feng, C. Yuan, W. Kong, B. Pan, J. Zhang and Y. Sun, *ChemCatChem*, **10**, 2078 (2018).
27. J. H. Oh, B. W. Kwon, J. Cho, C. H. Lee, M. K. Kim, S. H. Choi, S. P. Yoon, J. Han, S. W. Nam and J. Y. Kim, *Ind. Eng. Chem. Res.*, **58**, 6385 (2019).
28. E. I. Papaioannou, D. Neagu, W. K. W. Ramli, J. T. S. Irvine and I. S. Metcalfe, *Top. Catal.*, **62**, 1149 (2019).
29. G. S. Kim, B. Y. Lee, G. Accardo, H. C. Ham, J. Moon and S. P. Yoon, *J. Power Sources*, **423**, 305 (2019).
30. B. W. Kwon, J. H. Oh, G. S. Kim, S. P. Yoon, J. Han, S. W. Nam and H. C. Ham, *Appl. Energy*, **227**, 213 (2018).
31. G. S. Kim, B. Y. Lee, H. C. Ham, J. Han, S. W. Nam, J. Moon and S. P. Yoon, *Int. J. Hydrogen Energy*, **44**, 202 (2019).
32. A. Muñoz, G. Munuera, P. Malet, A. R. González-Elipe and J. P. Espinós, *Surf. Interface Anal.*, **12**, 247 (1988).
33. H. J. Borg, L. C. A. Van Den Oetelaar, J. W. Niemantsverdriet, *Catal. Lett.*, **17**, 81 (1993).
34. B. Faroldi, J. Múnera, J. M. Falivene, I. R. Ramos, Á. G. García, L. T. Fernández, S. G. Carrazán and L. Cornaglia, *Int. J. Hydrogen Energy*, **42**, 16127 (2017).
35. Z. L. Zhang, V. A. Tsipouriari, A. M. Efstathiou and X. E. Verykios, *J. Catal.*, **158**, 51 (1996).
36. D. A. J. M. Ligthart, R. A. Van Santen and E. J. M. Hensen, *J. Catal.*, **280**, 206 (2011).